CVEL

THE CLEMSON UNIVERSITY VEHICULAR ELECTRONICS LABORATORY

TECHNICAL REPORT: CVEL-17-069

Modeling a Multi-Layer Ceramic Capacitor with Losses Based on Physical Phenomena

J. Hunter Hayes and Dr. Todd Hubing

Clemson University

November 1, 2017

Table of Contents

Abstract

Multi-layer ceramic capacitors (MLCCs) in surface-mount packages are generally composed of a number of conducting plates stacked vertically. At high frequencies, when mounted on a printed circuit board, most of the current will only flow in the lower plates. The capacitor can be thought of as having a low-frequency equivalent circuit and a high-frequency equivalent circuit. Losses at lower frequencies are dominated by the dielectric. Losses at higher frequencies are dominated by skin effect losses in the electrodes. An eight-element circuit is proposed that models the behavior of surface-mount MLCCs over a wide band of frequencies.

1. Introduction

It can be beneficial to have access to a fast, accurate model of a multi-layer ceramic capacitor (MLCC). To better understand the behavior of a circuit utilizing an MLCC, the model of the MLCC should be based on what is physically happening in the body of the capacitor.

An MLCC can be difficult to model accurately because the effective resistance, capacitance, and inductance of the capacitor will vary with frequency [1]. Also, the internal inductance of the capacitor cannot be determined independently from the connection geometry.

Over the years, many models of MLCCs have been developed. Perhaps, the most common MLCC model is the series RLC circuit shown in Fig. 1. This model is commonly found in textbooks and capacitor datasheets.

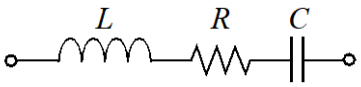

Fig. 1. Simple RLC model

The resistance in this model is referred to as the equivalent series resistance (ESR) of the capacitor, while the inductance represents the equivalent series inductance (ESL). The capacitance in this model is generally the nominal capacitance of the capacitor [2] – [3].

To increase the accuracy of the series RLC model, a resistance in parallel with the capacitance, which models the dielectric losses of the capacitor, is sometimes added [2] – [3]. This model is shown in Fig. 2 and will be referred to as an RLCR model.

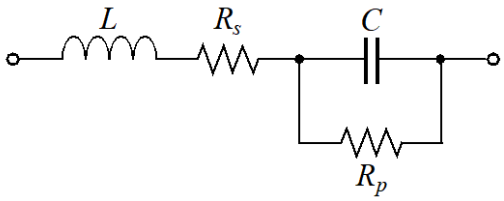

Fig. 2. RLC model with added parallel R

These models do a good job of modeling the gross behavior of MLCCs, but their accuracy is limited. The optimum value of each element in these models is frequency dependent. The model shown in Fig. 3 [4] – [6] adds additional elements to the RLC model in an attempt to increase the accuracy of the model over a wide range of frequencies. These added parameter values are generally determined through curve-

fitting to match measured data. This yields a very accurate model that is more complex than the RLC or RLCR models. Since the structure of the model is not based on the physical properties of the capacitor, this type of model is generally only useful for modeling the specific capacitor that was measured.

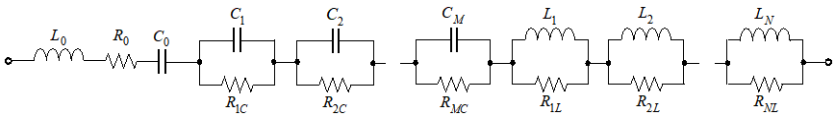

Fig. 3. Curve-fit model of MLCC

Fig. 4 shows a model developed by a capacitor manufacturer. This model is similar to the curve-fitted models discussed above but is much closer to representing the physical construction of the MLCC. In this model, there are many parallel RC branches mimicking the plate pairs of an MLC capacitor [7].

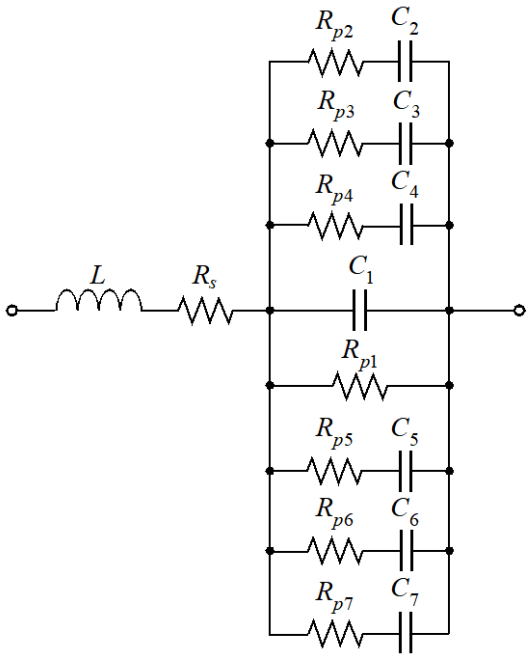

Fig. 4. Cap manufacturer model

Prymak developed the model of Fig. 5 and several derivatives for KEMET in [6], [8] – [9].

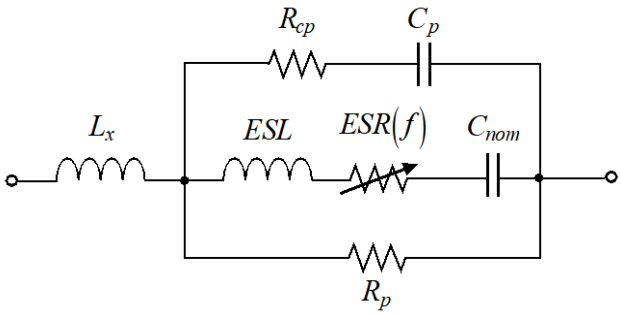

Fig. 5. Prymak model

This model is also based on the physical construction of the capacitor. Furthermore, it accounts for the frequency dependence of the resistance term, but the dependence is fit rather than attributed to any physical phenomena.

The model presented in Fig. 6 was developed by Smith and Hockanson in [10] – [11] and represents the stacked plate pairs of the MLCC. In the instance of the particular model shown in Fig. 6, the modeled capacitor contains ten plate pairs.

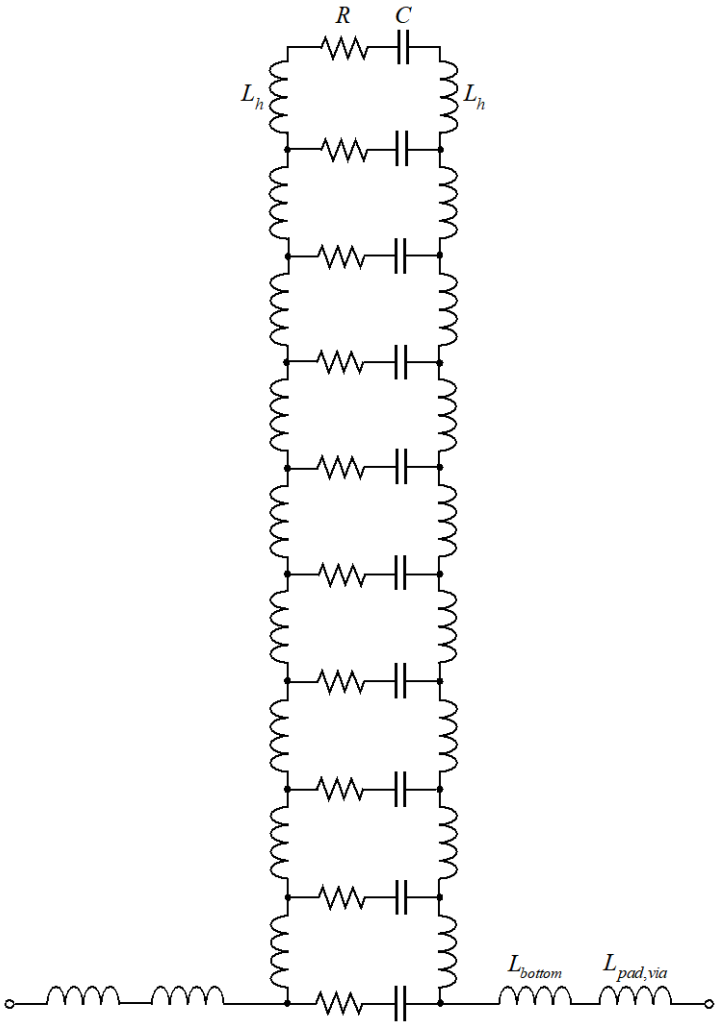

Fig. 6. Smith-Hockanson MLCC model

The model above uses parallel RC branches interconnected with inductance terms to model the plates of the capacitor. For every plate pair in the capacitor, there is an RC branch in the model. The inductance terms represent the partial inductances associated with getting current to the subsequent plate. Each branch uses the same parameter values because each plate of the capacitor has essentially the same geometry. The Smith-Hockanson model is based on the physical construction of the capacitor and is more accurate than the RLC or RLCR models; however, it is more complex.

Somewhat of a simplification of the models from [10] – [11], the model of [12], shown in Fig. 7, uses three RLC branches to model the MLCC. The authors show that a three-branch model provides improved accuracy over the single-branch RLC model without adding a large amount of complexity.

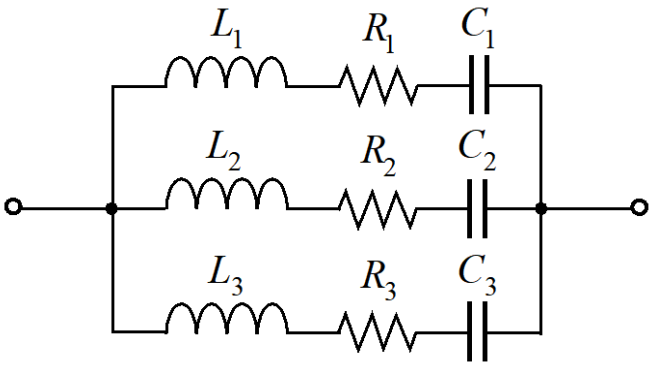

Fig. 7. Three-branch MLCC model

The model proposed in this paper more accurately describes the physical phenomena of an MLC capacitor. It is accurate over a broader frequency range than the simple models from [2] – [3], achieves this accuracy with minimal added complexity, and is simpler than many of the models proposed in [4] – [12].

2. Model Features

At low-frequencies, current will flow equally in all the plates of an MLCC; however it has been demonstrated in [13] – [15] that most of the high-frequency current in an MLCC flows on the lower plates of the capacitor when the current enters and exits the package from below. The transition occurs at frequencies where the impedance at the terminals of the capacitor is dominated by the inductance of the current path. Fig. 8 illustrates the paths that currents in a standard-electrode MLCC take at low and high frequencies.

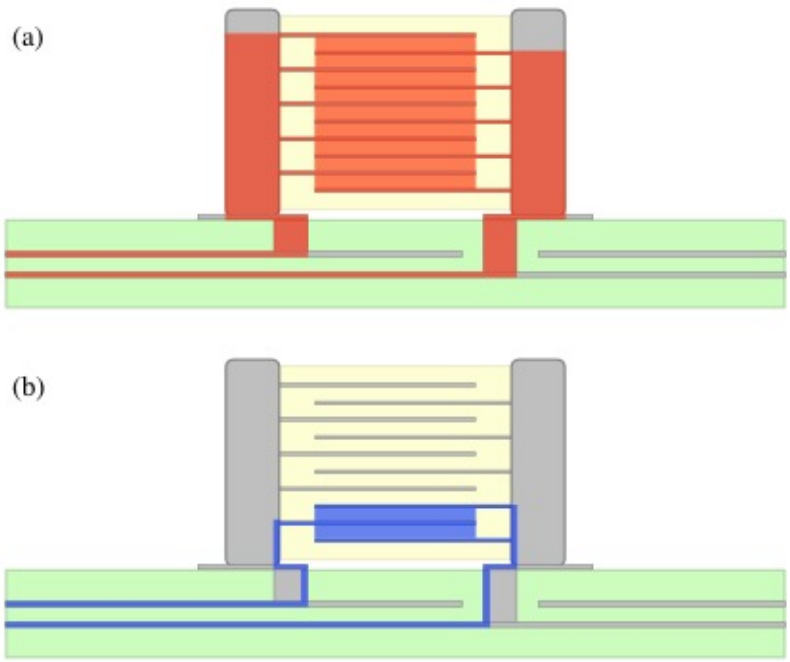

Fig. 8. Current path in a standard electrode MLCC at low frequencies (a) and high frequencies (b)

Another common configuration of MLCC is the floating-electrode design. Fig. 9 illustrates the current paths in a floating electrode MLCC at low and high frequencies. For capacitors with the same physical size and number of plate pairs, the electrode design will have an effect on the capacitor equivalent circuit parameters.

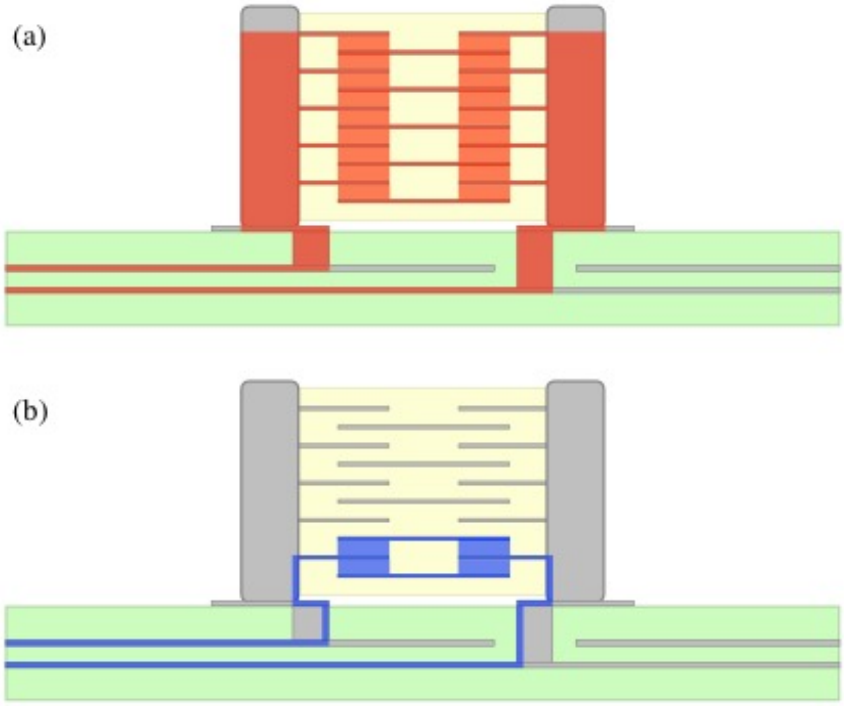

Fig. 9. Current path in a floating electrode MLCC at low frequencies (a) and high frequencies (b)

The proposed model for surface mount MLCCs has two branches: one branch represents an equivalent circuit at low frequencies, while the other branch represents the equivalent circuit at high frequencies. Together, the two branches model the MLCC over a broad frequency range. For ease of understanding, the branches will be referred to as the low-frequency branch and the high-frequency branch, respectively. For clarity, let the "self-resonant" frequency be defined as the frequency at which the primary LC resonance between the connection inductance and the nominal capacitance occurs.

The low-frequency branch is comprised of a series RLC circuit with a frequency-dependent resistance term. This resistance varies inversely with frequency and represents the dielectric losses, which are the dominant losses in an MLCC at lower frequencies [16] – [18]. The capacitance in the low-frequency branch will be a majority of the nominal capacitance, as it represents the capacitance of the plates that are not "seen" by high-frequency current. The inductance term of the low-frequency branch characterizes the inductance associated with the current path shown in Figs. 8a or 9a, depending on the capacitor electrode construction.

The high-frequency branch similarly consists of a series RLC circuit with a frequency-dependent series resistance term; however, the resistance term in this branch is proportional to the square root of frequency. This resistance simulates the skin effect losses of the plates, which are the dominant losses in the capacitor at high frequencies [16] – [17]. The capacitance of the high-frequency branch will be the capacitance of only one or two layers of the capacitor, since these are the layers that will carry the majority of the high-frequency current. The inductance of the high-frequency branch is that of the current path shown in Figs. 8b or 9b. The high-frequency inductance will be smaller than the low-frequency

inductance due to the smaller loop area associated with the high-frequency current path. The higher inductance of the low-frequency branch effectively forces high-frequency current to flow through the high-frequency branch. The inductance terms of both branches include the inductance associated with the connection to the capacitor, which will depend on the manner in which the capacitor is mounted to the circuit board. Because the two branch inductances will share most of the same loop area, there is a large mutual inductance between the inductance terms of the high- and low-frequency branches.

Two additional resistance terms are in series with the two branches of the model. One of these terms is constant while the other is proportional to the square root of the frequency. These resistances represent the constant and skin effect losses associated with the connection to the capacitor. Fig. 10 shows the proposed model of an MLC capacitor.

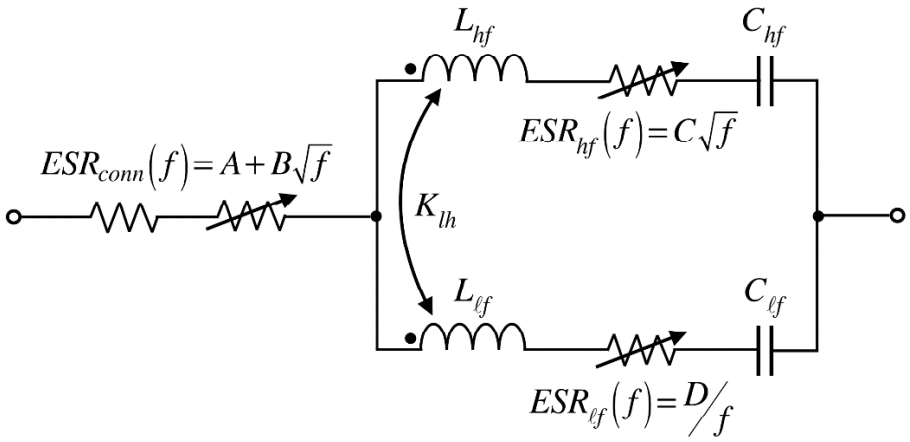

Fig. 10. Proposed MLCC model

At low frequencies, the ESR of the capacitor is dominated by the dielectric loss term found in the low-frequency branch. From [18], the relationship between ESR and dielectric loss is found to be

$$\mathrm{ESR} = \tan\delta \cdot \frac{1}{2\pi f C} \tag{1}$$

For cases where the dielectric loss is non-negligible, the ESR at low frequencies will naturally decrease with increasing frequency as described in (1). The impedance at low frequencies is dominated by the nominal capacitance.

At high frequencies, the ESR of the capacitor is dominated by the two skin effect terms, which are referred to as ESR_{conn} and ESR_{hf} in Fig. 10. The high-frequency impedance is dominated by the connection inductance of the capacitor.

3. MLCC Measurement Features

The ESR and impedance magnitude, |Z|, of X7R and NP0 MLC capacitors from three different manufacturers with a range of nominal capacitances were measured with an Agilent 4291B impedance analyzer connected to an Agilent 16092A test fixture. The available measurement frequency range of this combination is 1 to 500 MHz. Given the frequency limits of the measurement equipment, only capacitors with a nominal capacitance between 10 nF and 100 nF were evaluated, since these contained the primary features of interest in their impedance and ESR curves within this frequency range. Fig. 11 shows the equipment used to measure the capacitor properties.

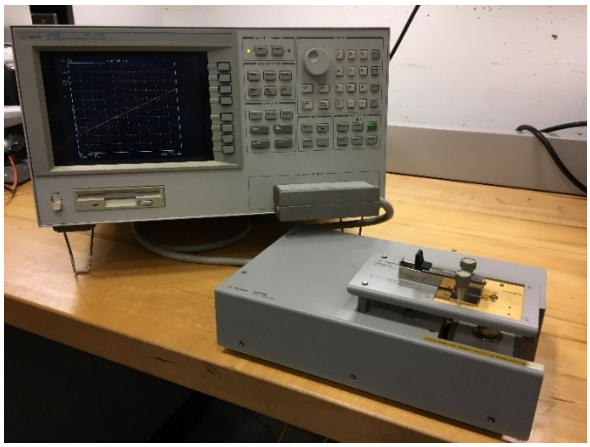

Fig. 11. Capacitor measurement setup

Fig. 12 shows the measured impedance of a typical 47-nF X7R capacitor. In this plot, the impedance at lower frequencies is that of the nominal capacitance. The connection inductance of the capacitor is dominant at higher frequencies. In between the two is the self-resonant frequency of the capacitor.

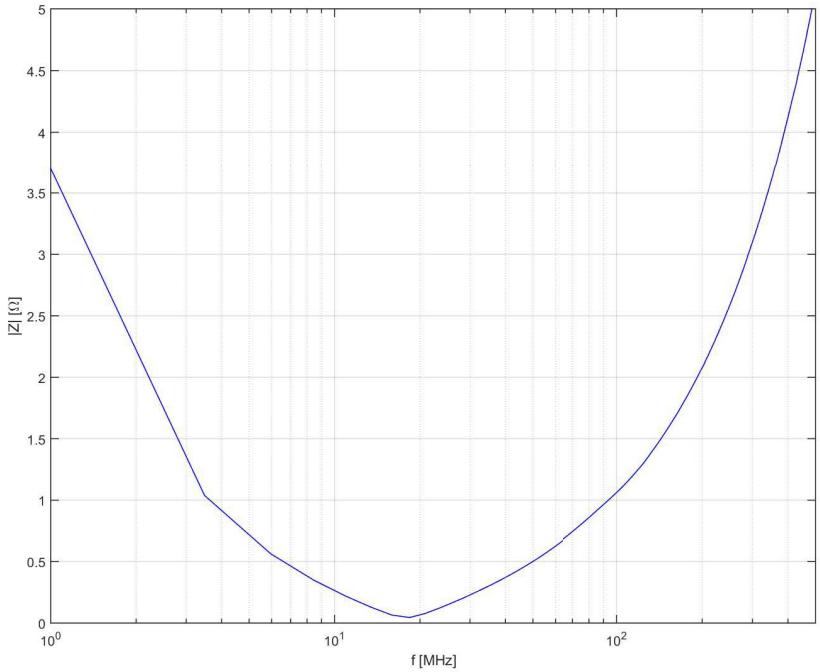

Fig. 12. Measured |Z| of a 47-nF X7R capacitor

A plot of the ESR of a typical 47-nF X7R capacitor is shown in Fig. 13. Like the impedance, the ESR of an MLCC can also be broken into two distinctive regions. At lower frequencies, the series losses are dominated by the losses in the dielectric of the capacitor. The dielectric losses are inversely proportional to frequency. At higher frequencies, the losses tend to be dominated by skin effect losses in the capacitor plates which are proportional to the square root of frequency. The ESR curve exhibits a resonance between the two regions, around 100 MHz in Fig. 13, which is caused by internal resonances within the body of the capacitor.

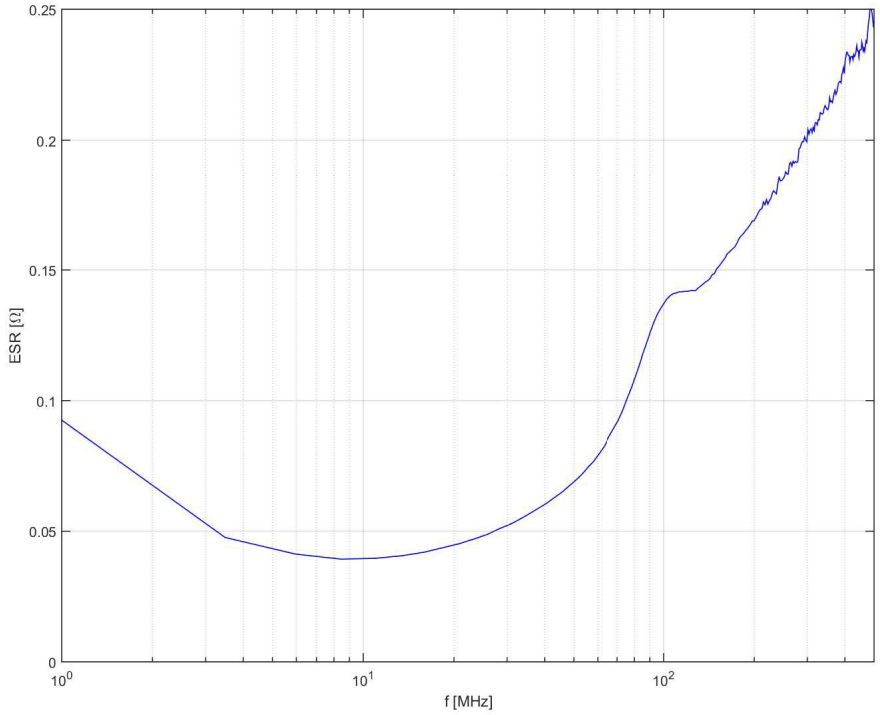

Fig. 13. Measured ESR of a 47-nF X7R capacitor

The lossiness of the dielectric also plays a large role in determining the overall characteristics of the ESR curve. In Fig. 14, the ESR of a typical 47-nF X7R capacitor is compared to that of a typical 47-nF NP0 capacitor from the same manufacturer.

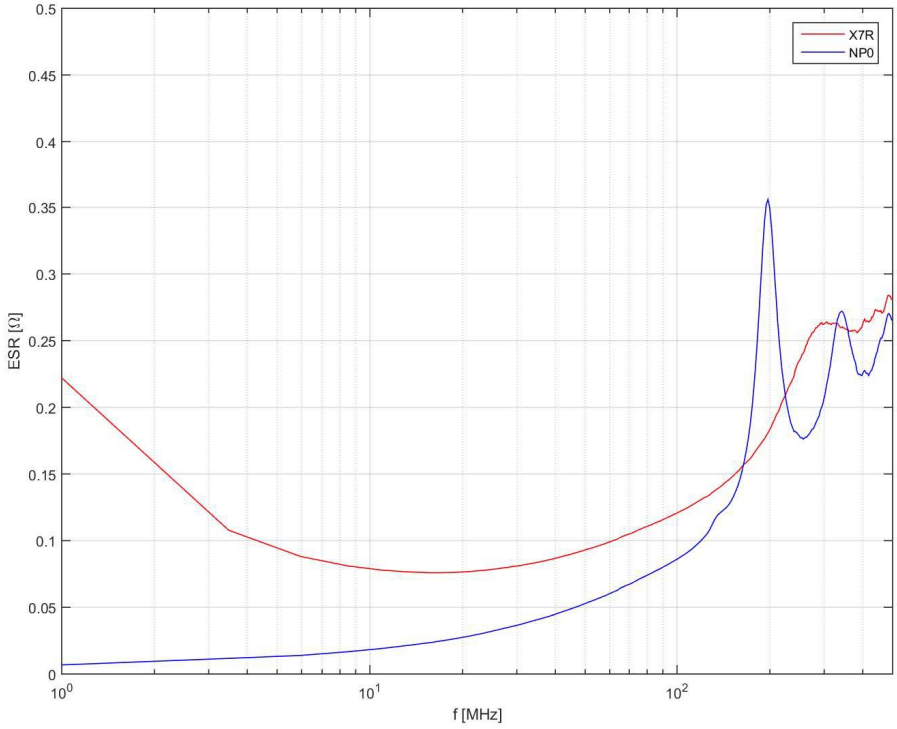

Fig. 14. Comparison of measured ESR for 47-nF X7R and NP0 capacitors

The X7R dielectric is more lossy than NP0. One direct effect of the lossiness of the dielectric to the ESR curve is the value of ESR at low frequencies. From Fig. 14, the lossier dielectric, X7R, has much higher losses at low frequencies. From (1), it is expected that the ESR of a dielectric with negligible dielectric loss will not show a strong frequency-dependence at lower frequencies where dielectric losses are dominant. This is reflected in Fig. 14 in the ESR of the NP0 capacitor.

In addition to affecting the low-frequency ESR, the lossiness of the dielectric plays a role in determining the damping of the transition between the two major regions of the ESR curve. Fig. 14 shows resonances in both X7R and NP0 ESR curves around 200–300 MHz; however, the resonances in the ESR curve of the NP0 capacitor have much lower damping than those in the ESR curve of the X7R capacitor. Also, the NP0 ESR curve clearly contains multiple resonances in this region whereas the X7R curve only displays one. The author speculates that these resonances are due to internal resonances within the body of the capacitor.

4. Comparison with Measured Data

To evaluate the accuracy and physical relevance of the model from Fig. 10, three different X7R capacitors were selected such that the package size and spacing between layers were the same. The nominal capacitances selected were 10, 47, and 100 nF. All three capacitors selected were produced by the same manufacturer.

Fig. 15 shows the proposed model of a 10-nF X7R capacitor.

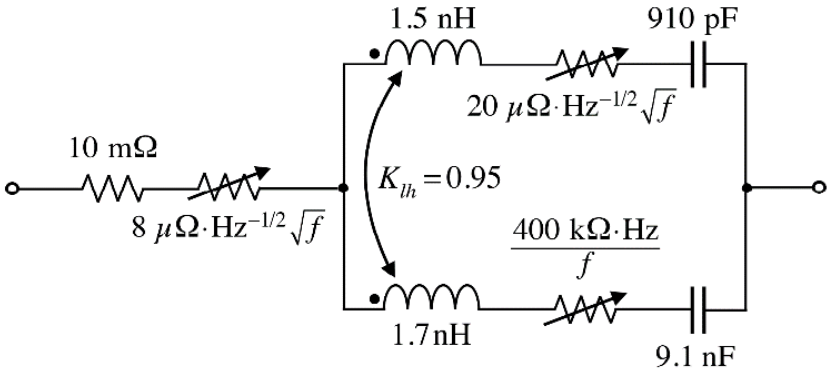

Fig. 15. Proposed model of 10-nF X7R MLC capacitor

According to the manufacturer, the 10-nF X7R capacitor has an approximate capacitance per layer of 454 pF and is comprised of 22 active layers. Given the assumption that high-frequency current only flows in a couple of layers, the capacitance of the high-frequency branch of the model was determined by doubling the single-layer capacitance. Consequently, the low-frequency branch capacitance was determined to be the remainder of the nominal capacitance. The mutual inductance between the loops was estimated to be 0.95 due to most of the loop area being shared by both branches. The package size, estimated loop area, and capacitor self-resonant frequency were used to estimate the inductance terms. The low-frequency inductance was first determined, and the high-frequency inductance was selected to be slightly less than the low-frequency inductance. The dielectric loss term was selected to provide good agreement with the measured data. The constant series resistance of the electrodes was estimated to be 10 mΩ. Both of the skin effect terms were determined by adjusting their constant while comparing to the modeled data.

ESR and impedance plots were generated for the model of Fig. 15 and were compared to measured data. In Fig. 16, the measured ESR of a 10-nF, X7R capacitor is compared with the ESR generated by the SPICE model of Fig. 15.

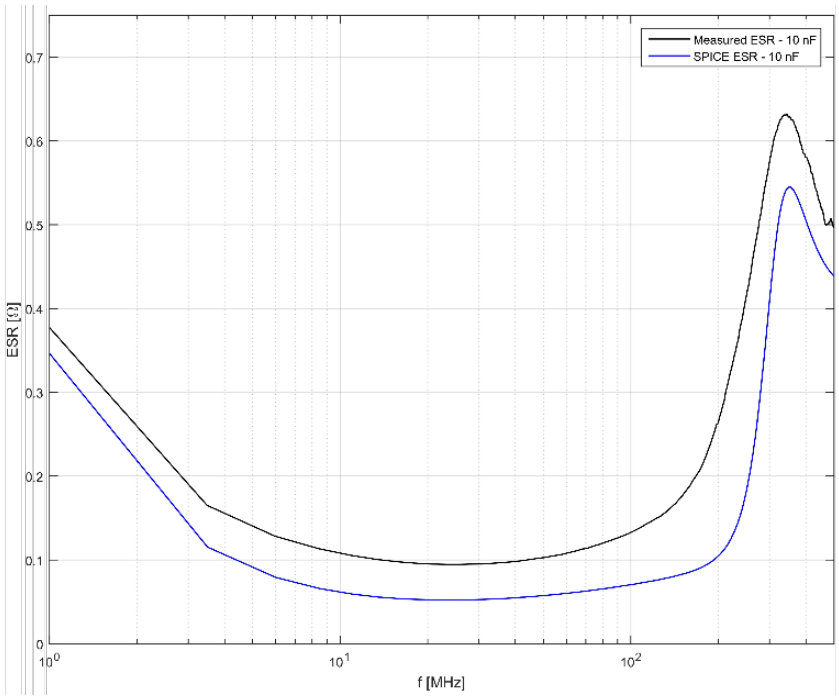

Fig. 16. Comparison of measured ESR with that of a SPICE model for a 10-nF X7R capacitor

While the accuracies of each SPICE model could be improved upon what is presented here, the accuracies of the individual models were sacrificed for improved accuracy across all three models with parameter differences between the three models consistent with the physical differences between the three capacitors.

Throughout the measured frequency range, the SPICE model is on average within 35% of the measured ESR of the 10-nF, X7R capacitor. At worst, around 200 MHz, the agreement is within 60% of the measured value.

It was found that the model without mutual inductance frequently over-predicted the ESR at the resonance around 350 MHz in Fig. 16. When the mutual inductance term was added, the agreement at this resonance was improved for all modeled capacitors.

Fig. 17 shows the measured |Z| of a 10-nF, X7R capacitor compared to the |Z| of the SPICE model from Fig. 15.

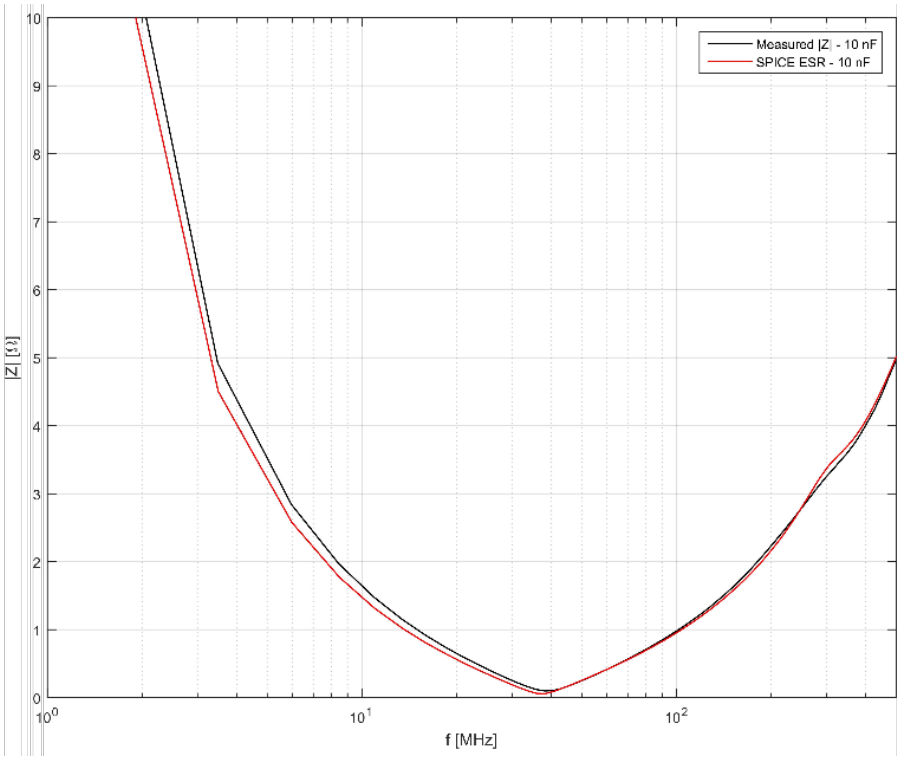

Fig. 17. Comparison of measured |Z| with that of a SPICE model for a 10-nF X7R capacitor

In Fig. 17, there is a slight resonance in the |Z| plot around 300 MHz. This echoes the much larger resonance seen in the ESR plot of Fig. 16. The authors suspect that this resonance in the |Z| plot is due to internal resonances and is generally damped by the mutual inductance of the capacitor plates and other losses within the capacitor. The mutual inductance of the capacitor plates opposes the flow of circulating currents between the plates of the capacitor and thus damps any internal resonances that occur. The model slightly exaggerates the resonance seen in the measured data, but apart from this and a slight error in the self-resonant frequency, the model accurately predicts the |Z| of the measured capacitor.

Fig. 18 shows the SPICE model of a 47-nF X7R capacitor. The 47-nF capacitor assessed has an approximate capacitance per layer of 2.04 nF and is comprised of 23 active layers. Thus, using the same assumption as with the 10-nF model, the high frequency capacitance is twice the single-layer capacitance and the low-frequency capacitance is the remainder of the nominal capacitance. Since the number of layers is nearly the same as that of the 10-nF capacitor, the inductance of the high- and low-frequency branches and the mutual inductance between them remains unchanged from the 10-nF model. Since there is no difference between the end electrodes, there is also no change to the resistance terms in series with both branches.

It was observed that dielectric losses decrease with increasing nominal capacitance for the X7R capacitors evaluated. This is predicted by (1). Due to this effect, the dielectric loss term of the 47-nF capacitor model is lower than that of the 10-nF model. Since the high-frequency model still assumes that high-frequency current is flowing in the same number of plates, the skin effect losses in the high-frequency branch will be the same as those in the 10-nF model. The proposed model for a 47-nF, X7R capacitor is shown in Fig. 18.

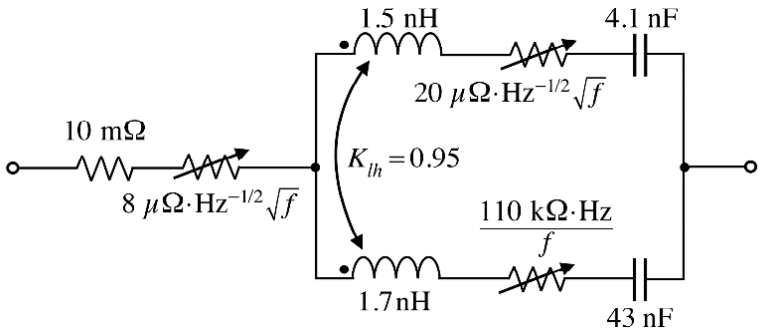

Fig. 18. Proposed SPICE model of a 47-nF X7R MLC capacitor

The modeled ESR is compared to the measured ESR of a 47-nF, X7R capacitor in Fig. 19. For this capacitor, the model accurately predicts the behavior of the measured ESR at low frequencies. At higher frequencies, the model overestimates the losses, but is within one-and-a-half times the measured ESR.

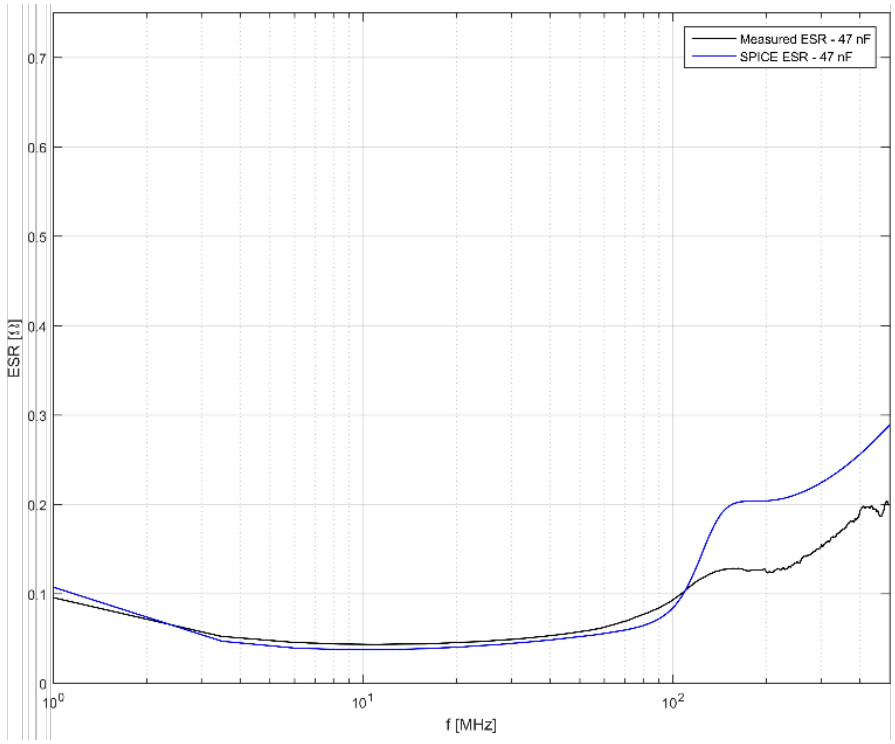

Fig. 19. Comparison of measured ESR with that of a SPICE model for a 47-nF X7R capacitor

Fig. 20 compares the modeled |Z| to measured |Z| for the 47-nF, X7R capacitor. The agreement between measured and modeled impedance curves in Fig. 20 is good.

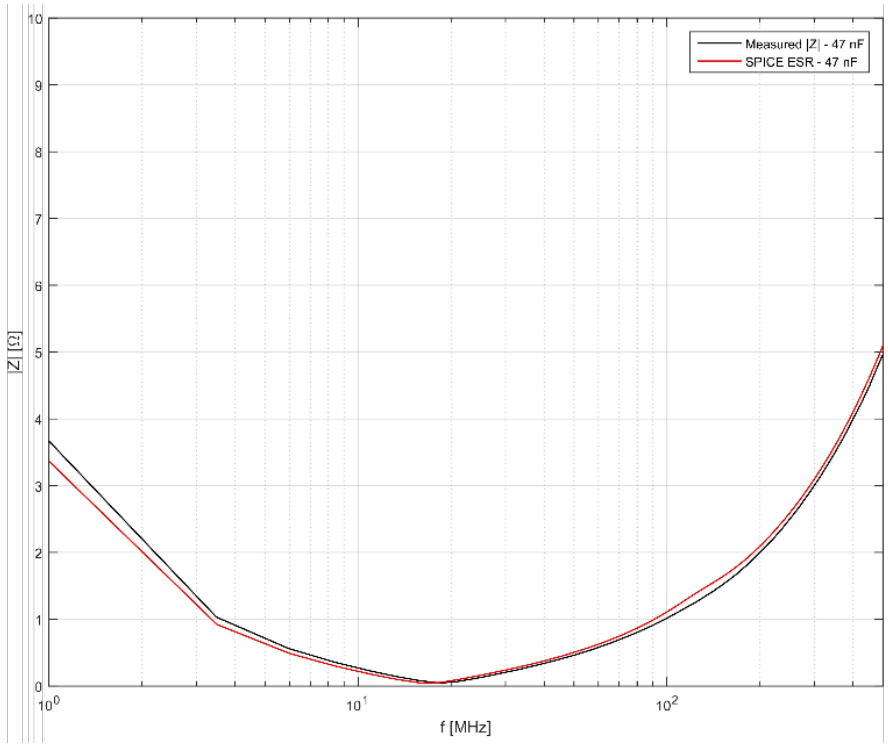

Fig. 20. Comparison of measured |Z| with that of a SPICE model for a 47-nF X7R capacitor

The 100-nF capacitor selected has a capacitance per layer of 37 nF and is comprised of 37 active layers. Thus, the low-frequency inductance is lower than the other capacitors modeled because there are more plates in parallel. With more plates in the stackup but a comparable package height, the lower plates will be closer to the bottom of the capacitor body [19]. This causes the high-frequency inductance to also be lower than the other capacitors modeled. As with the models of the other two capacitors, the high-frequency capacitance is twice the single-layer capacitance, and the low-frequency capacitance is the remainder of the nominal capacitance. Since a similar amount of loop area is shared between the two current paths, there is no change in mutual inductance from that of the other two models. Like the difference between the 10-nF model and the 47-nF model, the dielectric losses of the 100-nF capacitor will be lower than those of the 47-nF capacitor. Again, there is no change to the resistance terms in series with both branches. Fig. 21 shows the proposed SPICE model for a 100-nF, X7R capacitor.

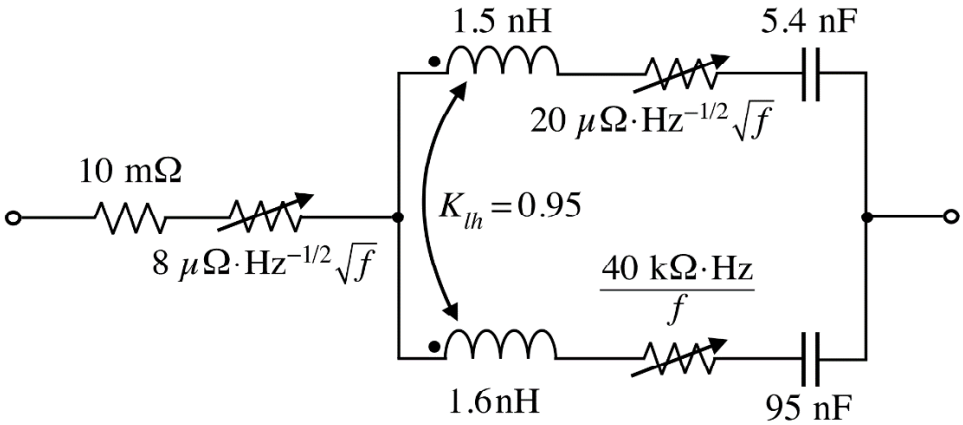

Fig. 21. Proposed model of a 100-nF X7R MLC capacitor

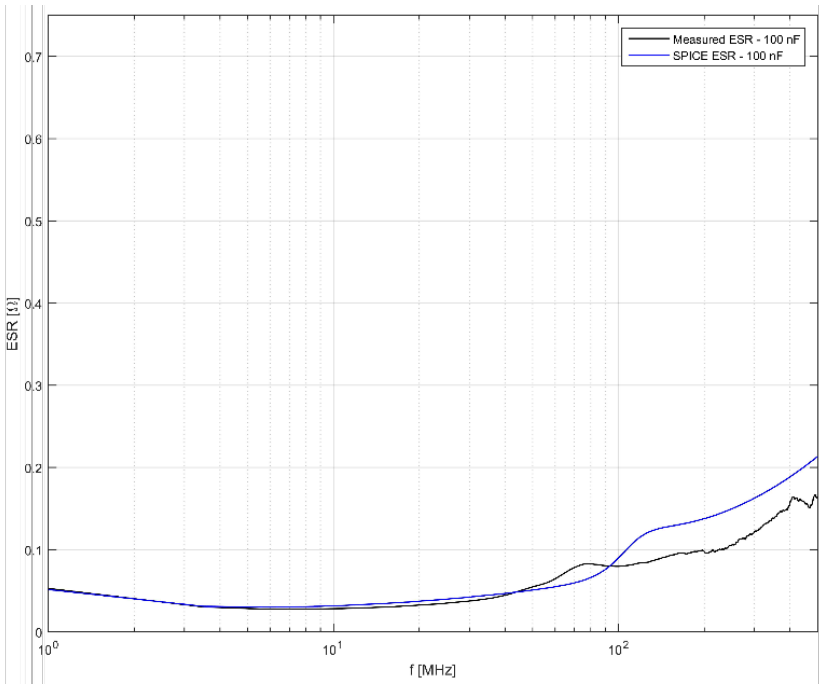

Fig. 22. Comparison of measured ESR with that of a SPICE model for a 100-nF X7R capacitor

Similar to the ESR of the 47-nF capacitor, Fig. 22 shows that the model of the 100-nF capacitor matches the measured data very well at low frequencies, but overestimates within one-and-a-half times the ESR at high frequencies.

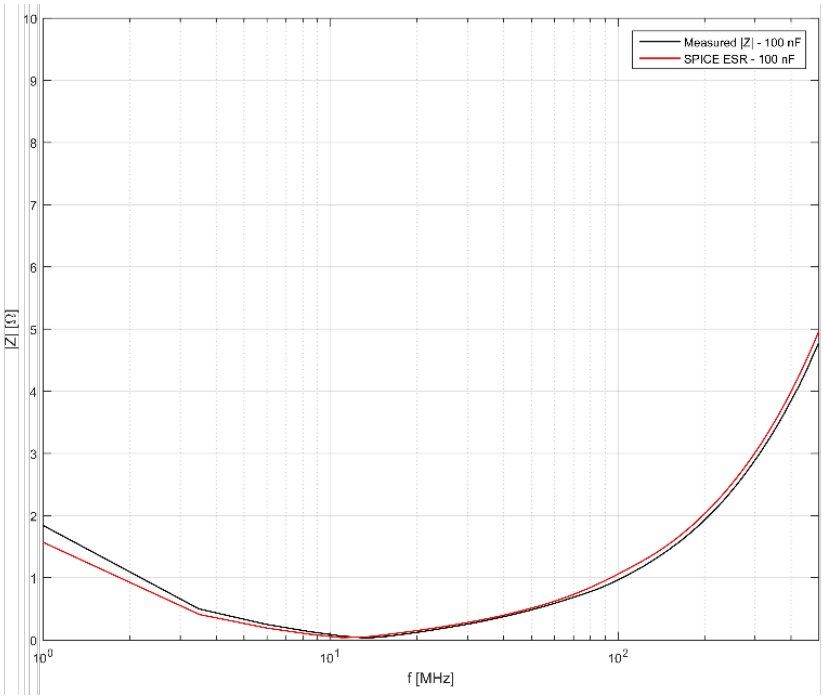

Fig. 23. Comparison of measured |Z| with that of a SPICE model for a 100-nF X7R capacitor

Also, like the 47-nF capacitor, Fig. 23 shows an accurate prediction of the |Z| for all the measured frequency range.

5. Conclusion

The model proposed in this paper demonstrates a simple yet accurate way of modeling the impedance and series resistance of surface-mount multi-layer ceramic capacitors. The proposed model is based on physical phenomena. The model accounts for the transition from low frequencies where the current flows equally in all plates to high frequencies where current flows primarily in the lower plates. At lower frequencies, frequency-dependent dielectric losses dominate the ESR. Conversely, at higher frequencies, frequency-dependent skin effect losses are dominant. The model provides a natural transition between these two forms of loss by way of its two branches and their differing inductances. Mutual inductance between the two branches, caused by the shared loop area between high- and low-frequency currents, helps damp the internal resonance observed in both the model and measurements.

Measurements of the impedance magnitude and ESR of 10-, 47-, and 100-nF X7R capacitors were taken and compared to modeled data. This paper demonstrates that the proposed model closely matches measured data for several X7R capacitors with differing nominal capacitances. Thus, the proposed two-branch model with mutual inductance and frequency-dependent resistances provides an effective way of modelling multi-layer ceramic capacitors while accounting for the physical phenomena that contribute to losses.

References

[1] I. Novak and J. R. Miller, "Frequency-Dependent Characterization of Bulk and Ceramic Bypass Capacitors," *Proc. Topical Meeting Electrical Performance Electron. Packag.*, Princeton, NJ, Oct. 2003.

[2] C. R. Paul, *Introduction to Electromagnetic Compatibility, 2nd ed.*, Hoboken, NJ, USA: Wiley, 2006.

[3] Equivalent Circuit Model Library, TDK, Automotive Grade CGA3 Series.

[4] C.C. Kuo, M. Y. Kuo, and M. S. Kuo, "Modeling of Capacitors and Nonlinear Inductors Using Piecewise Curve Fitting Technique," *IEEE Workshop on Computers in Power Electronics*, Trois-Rivieres, Que., Aug. 1994, pp. 133–138.

[5] J. Lu and L. Ou, "Modeling Ceramic and Tantalum Capacitors by Automatic SPICE Parameter Extractions," *IEEE Applied Power Electronics Conference and Exposition*, Mar. 2005, vol. 3, pp. 6–10.

[6] J. Prymak et al., "Capacitor EDA Models with Compensation for Frequency, Temperature, and DC Bias," *Proc. Capacitor and Resistor Technology Symposium*, CARTS Conference, New Orleans, LA, Mar. 2010.

[7] TDK Corporation. (2017, October 8). SPICE Netlist (Precision) for CGA3E2X7R1H102K080AA. [Online]. https://product.tdk.com/info/common/tvcl/capacitor/ceramic/mlcc/spice_p/CGA3E2X7R1H102K080AA_p.mod

[8] J. D. Prymak, "SPICE Modeling of Capacitors," Capacitor and Resistor Technology Symposium *Proceedings, CARTS Conference*, Mar. 1995.

[9] "Modeling a Capacitor," *Intusoft Newsletter*, Issue V44, Nov. 1995.

[10] L. D. Smith and D. Hockanson, "Distributed SPICE circuit model for ceramic capacitors," in *Proc. 51st Electron. Comp. Technol. Conf.*, Orlando, FL, May–Jun. 2001, pp. 523–528.

[11] L. D. Smith, D. Hockanson, and K. Kothari, “A Transmission-Line Model for Ceramic Capacitors for CAD Tools Based on Measured Parameters,” in *Electron. Compon. Technol. Conf.*, 2002, pp. 331–336.

[12] L. E. Wojewoda et al., “Use Condition Characterization of MLCCs,” *IEEE Trans. On Advanced Packaging*, vol. 32, no. 1, pp. 109–115, Feb. 2009.

[13] J. Kwak et al., “Plate Orientation Effect on the Inductance of Multi-Layer Ceramic Capacitors,” *Proc. IEEE Electrical Performance of Electronic Packaging,* Atlanta, GA, Oct. 2007, pp. 95–98.

[14] Z. Yang et al., “Inductance of Bypass Capacitors: How to Define, How to Measure, How to Simulate,” DesignCon 2005, TecForum TF7, 2005.

[15] J. M. Hock et al., “Inductance of Bypass Capacitors: How to Define, How to Measure, How to Simulate,” DesignCon East, TecForum TF-MP2, 2005.

[16] I. Novak, “How to read the ESR curve,” QuietPower: PCB Design 007, Oct. 2012.

[17] Murata Manufacturing Co., Ltd. (2017, October 8). What are impedance/ESR frequency characteristics in capacitors?. [Online]. http://www.murata.com/en-us/products/emiconfun/capacitor/2013/02/14/en-20130214-p1

[18] A.C. Lynch, “Relationship between permittivity and loss tangent,” *Proc. IEE*, vol. 118, no. 1, pp. 244–246, Jan. 1971.

[19] M. Laps, private communication, Nov. 2016.